

# Cohesive versus overlapping crack model for a size effect analysis of RC elements in bending

A. Carpinteri, M. Corrado, M. Paggi & G. Mancini

*Department of Structural and Geotechnical Engineering, Politecnico di Torino, Italy*

**ABSTRACT:** The well-known *Cohesive Crack Model* describes strain localization with a softening stress variation in concrete members subjected to tension. An analogous behaviour is also observed in compression, when strain localization takes place in a damaged zone and the stress reaches the compressive strength with surface energy dissipation. In the present paper, we propose the new concept of *Overlapping Crack Model*, which is analogous to the cohesive one and permits to simulate material compenetration.

The two aforementioned elementary models are merged into a more complex algorithm able to describe both cracking and crushing growths during loading processes in RC members. A numerical procedure based on elastic coefficients is developed, taking into account the proposed constitutive laws in tension and compression. With this algorithm, it is possible to effectively capture the flexural behaviour of RC beams by varying the reinforcement percentage and/or the beam depth.

## 1 INTRODUCTION

The description of the behaviour of reinforced concrete members is complicated by the contemporaneous presence of different nonlinear contributions: crack opening in tension, concrete crushing in compression and steel yielding or slippage.

In most practical applications, the concrete contribution in tension is totally neglected or just considered with a linear-elastic stress-strain law until the ultimate tensile strength is reached. The nonlinear concrete behaviour in compression is certainly not negligible. Many different laws may be used to model the concrete behaviour in compression: elastic-perfectly plastic, parabolic-perfectly plastic, Sargin's parabola, etc. The most utilised constitutive laws for steel are the elastic-perfectly plastic or the elastic-hardening stress-strain relationships. Using these constitutive laws with a FEM program, it is possible to fully describe the behaviour of a reinforced concrete member, though it is difficult to catch the size-scale effects. The reason is that the above-mentioned constitutive laws consider only an energy dissipation over the volume in the nonlinear regime.

On the other hand, the application of Fracture Mechanics concepts has been proved to be very effective for the analysis of size-scale effects. In particular, Carpinteri (1986) proposed a cohesive formulation to explain the ductile-brittle transition in

unreinforced concrete beams under three-point bending test. This algorithm can also be used to describe the nonlinear behaviour of concrete in RC members.

With regard to the behaviour of concrete in compression, Hillerborg (1990) firstly introduced a model based on the concept of strain localization. According to his approach, when the ultimate compressive strength is achieved, a strain localization takes place within a characteristic length proportional to the width of the compressed zone. This model permits to study the problem of size effects, although the definition of the length over which the strain localization occurs is not clear.

Furthermore, many experimental tests, see e.g. Van Vliet and Van Mier (1996), Carpinteri et al. (2005), Suzuki et al. (2006) put into evidence that a significant scale effect on dissipated energy density takes place. This parameter can be assumed as a material constant only if it is defined as a crushing surface energy. Hence, it emerges that the process of concrete crushing can be analysed with an approach similar to the cohesive model, which is valid for the tensile behaviour of concrete. In particular, we can define a linear-elastic stress-strain law, before achieving the compressive strength. Afterwards, a descending stress-displacement law can be introduced, for the analysis of the nonlinear behaviour in compression.

Finally, a special mention has to be given to the steel-concrete interaction. The most appropriate law for the reinforcing bar bridging a tensile crack propagating in concrete is a nonlinear relationship between force and crack opening. For this reason, it is appropriate to consider a bond-slip law characterizing the interaction between steel and concrete.

In the next sections we propose a method able to describe step-by-step the behaviour of a reinforced concrete member during both fracturing and crushing. Firstly, we introduce separately the elementary models that we use to describe the whole concrete behaviour: the *Cohesive Crack Model* for concrete in tension, the *Overlapping Crack Model* for concrete in compression, and the stress-displacement relationship for steel in tension. A closed-form solution is also proposed to demonstrate that the strain localization in compression causes ductile-brittle transition by varying the structural dimension. Finally, the proposed numerical algorithm and some applications are reported to investigate on the influence of the various model's parameters.

## 2 MATHEMATICAL FORMULATION

Let us consider the reinforced concrete member shown in Fig. 1, subjected to a bending moment  $M$ . We assume that the midspan cross-section is fully representative of the mechanical behaviour of the whole element. The stress distribution is linear-elastic until the tensile stress at the intrados achieves the concrete tensile strength. When this threshold is overcome, a cohesive crack propagates from the bottom side toward the upper side. Correspondingly, the applied moment increases. Outside the crack, the material is assumed to behave elastically (Fig. 2). The stresses in the cohesive zone depend on the crack opening displacement and become equal to zero when the crack opening reaches a critical value and beyond.

On the other hand, concrete crushing takes place when the maximum stress in compression reaches the concrete compressive strength. Damage is described as a compenetration between the two half-beams representing the cause of the localization of the dissipated energy (Fig. 3). Larger the compenetration, also called *overlapping*, lower the transferred forces along the damaged zone.

### 2.1 Cohesive Crack Model

Linear Elastic Fracture Mechanics has been proven to be a useful tool for solving fracture problems, provided that a crack-like notch or flaw exists in the body and that the nonlinear zone ahead of the tip is negligible. These conditions are not always fulfilled and, both for metallic and cementitious materials, the size of the nonlinear zone due to plasticity or mi-

crocracking may be not negligible with respect to other dimensions of the cracked geometry. The localized damaged material may be modelled as a pair of restrained fracture surfaces. This idea has been extensively applied to materials which are commonly classified as quasi-brittle such as concrete, glass, polymers, rocks, etc. In particular, the most suitable model for concrete was firstly proposed by Hillerborg et al. (1976) with the name of *Fictitious Crack Model*. Carpinteri (Carpinteri et al. (1985) and Carpinteri (1989a)), introduced the terminology *Cohesive Crack Model* and applied an updated algorithm to the study of ductile-brittle transition and snap-back instability in concrete.

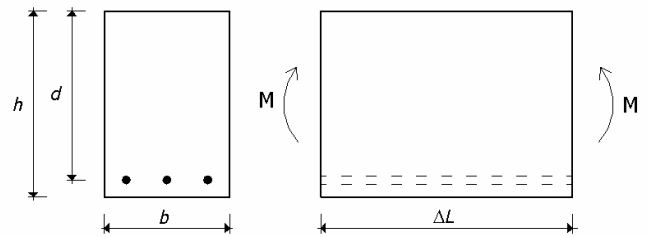


Figure 1. Scheme of a reinforced concrete element.

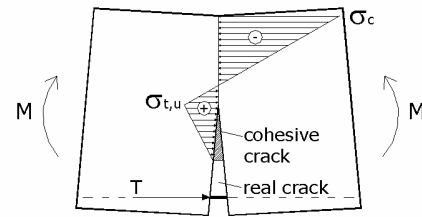


Figure 2. Cohesive stress distribution in tension with linear-elastic distribution in compression.

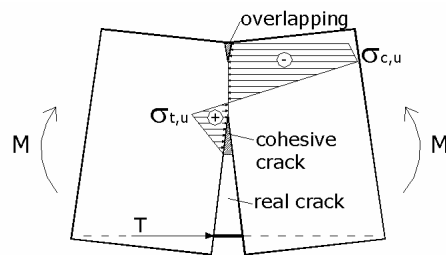


Figure 3. Nonlinear behaviour in tension and compression.

The hypotheses of the model can be summarized as follows:

- (1) The constitutive law used for the non-damaged zone is the  $\sigma$ - $\varepsilon$  linear-elastic law shown in Fig. 4a.
- (2) The process zone develops when the maximum stress reaches the ultimate tensile strength.
- (3) The process zone is perpendicular to the main tensile stress.
- (4) In the process zone, the damaged material is still able to transfer a tensile stress across the crack surfaces. The cohesive stresses are considered as de-

creasing functions of the crack opening  $w^t$ , (see Fig. 4b):

$$\sigma_t = \sigma_{t,u} \left( 1 - \frac{w^t}{w_c^t} \right), \quad (1)$$

where  $w^t$  is the crack opening,  $w_c^t$  is the critical value of the crack opening and  $\sigma_{t,u}$  is the ultimate tensile strength of concrete.

The shaded area under the stress vs. displacement curve in Fig. 4b represents the fracture energy,  $\mathcal{G}_F^t$ .

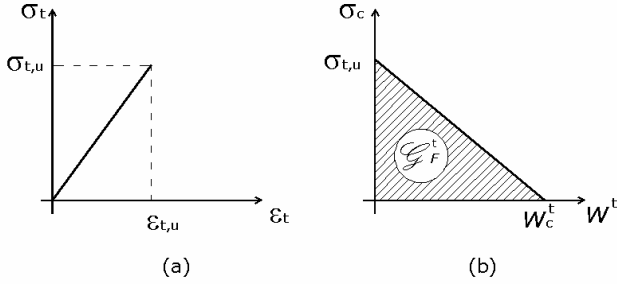


Figure 4. Concrete constitutive laws in tension: linear-elastic (a); post-peak softening (b).

## 2.2 Overlapping Crack Model for concrete crushing

The most frequently adopted constitutive laws for concrete in compression describe the material behaviour in terms of stress and strain. This approach imply that the energy is dissipated over a volume, whereas experimental results reveal that the energy is mainly dissipated over a surface. Hillerborg (1990) firstly proposed to model the crushing phenomenon as a strain localization over a length proportional to the depth of the compressed zone. However, the evaluation of this characteristic length is rather complicated by the fact that the depth of the compressed zone varies during the loading process. As a result, it is difficult to formulate a material constitutive law describing the mechanical response of concrete in compression.

In our formulation, we introduce a stress-displacement relationship between the compressive stress and the compenetrations, in close analogy with the cohesive model. The main hypotheses are the following:

(1) The constitutive law used for the undamaged material is a linear-elastic stress-strain relationship, see Fig. 5a.

(2) The crushing zone develops when the maximum compressive stress achieves the material strength for concrete.

(3) The process zone is perpendicular to the main compressive stress.

(4) The damaged material in the process zone is

assumed to be able to transfer a stress between the overlapping surfaces. Concerning the crushing stresses, they are assumed to be a decreasing function of the compenetrations  $w^c$  (Fig. 5b):

$$\sigma_c = \sigma_{c,u} \left( 1 - \frac{w^c}{w_c^c} \right), \quad (2)$$

where  $w^c$  is the compenetrations,  $w_c^c$  is the critical value of overlapping and  $\sigma_{c,u}$  is the ultimate compressive strength. This zone is represented by a fictitious overlapping, that is analogous to the fictitious crack in tension, as shown in Fig. 6.

In analogy with the cohesive crack model, we can define the area under the stress-displacement curve as the crushing energy,  $\mathcal{G}_F^c$ .

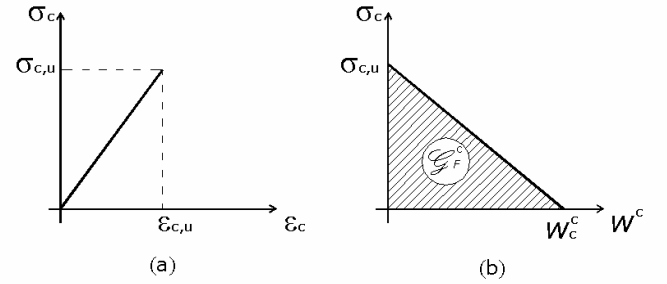


Figure 5. Concrete constitutive laws in compression: linear-elastic (a); post-peak softening (b).

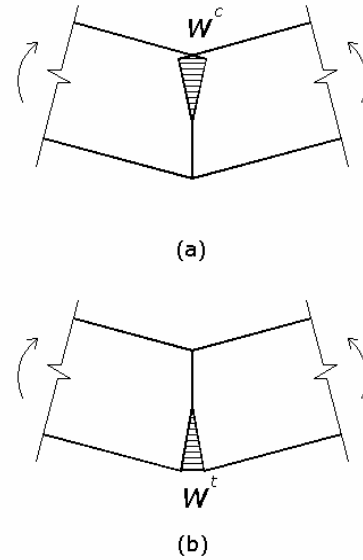


Figure 6. Compression crushing with overlapping (a); tensile fracture with cohesive zone (b).

A more sophisticated stress-displacement law considering the phenomenon of compacting, was recently proposed by Suzuki et al. (2006). In this case, the crushing energy is computed according to the following empirical equation, which considers the confined concrete compressive strength, by means of the stirrup yield strength and the stirrup volumetric

content:

$$\frac{\mathcal{G}_F^c}{\sigma_{c,0}} = \frac{\mathcal{G}_{F,0}^c}{\sigma_{c,0}} + 10000 \frac{k_a^2 p_e}{\sigma_{c,0}^2}. \quad (3)$$

Parameter  $\mathcal{G}_{F,0}^c$  is the crushing energy for unconfined concrete,  $\sigma_{c,0}$  is the average compressive strength,  $k_a$  is the parameter depending on the stirrup strength and ratio and  $p_e$  is the effective lateral pressure.

A comparison between the crushing energy and the fracture energy for different compressive strengths is proposed in Tab. 1. The crushing energy is calculated according to Eq. (3) for concrete without stirrups, while the fracture energy is calculated according to the CEB-FIP Model Code 90 in case of maximum aggregate dimension of 16 mm. It is worth noting that  $\mathcal{G}_F^c$  is between 2 and 3 orders of magnitude higher than  $\mathcal{G}_F^t$ .

Finally, we remark that the critical values for crushing compenetration and crack opening are respectively  $w_c^c \approx 1$  mm and  $w_c^t \approx 0.1$  mm.

Table 1. Comparison between crushing energy and fracture energy for different concrete compressive strengths.

$\sigma_{c,0}$	$\mathcal{G}_F^c$	$\mathcal{G}_F^t$
N/mm <sup>2</sup>	N/mm	N/mm
30	30	0,065
50	40	0,090
70	51	0,117
90	58	0,140

### 2.3 Steel-Concrete interaction

In order to model the steel contribution to the load carrying capacity of the beam, it is necessary to introduce a suitable bond-slip law for the characterization of steel-concrete interaction. Typical bond-slip relationships are defined in terms of a tangential stress along the steel-concrete interface as a function of the relative tangential displacement between the two materials (see Jenq and Shah (1989), Model Code 1990, Carpinteri (1999)). The integration of the differential slip over the transfer length,  $l_{tr}$ , is equal to half the opening crack at the reinforcement level, as shown in Fig. 7a. On the other hand, the integration of the bond stresses gives the reinforcement reaction. In order to simplify the calculation, the stress-displacement law is assumed to be linear until the yield stress (or until the critical opening crack for steel  $w_c^y$ ) is achieved. After that, the reinforcement reaction is considered as constant (Fig. 7b).

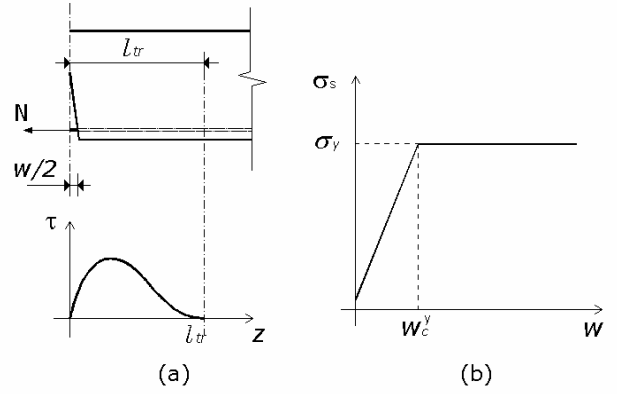


Figure 7. Bond stresses  $\tau$  in the transfer length  $l_{tr}$  (a); stress-displacement law for steel (b).

### 3 PURE CRUSHING COLLAPSE

Let us consider a reinforced concrete beam under three-point bending. We assume a rigid-perfectly plastic constitutive law for steel, whereas for concrete we use the constitutive law shown in Fig. 5. The linear elastic behaviour, with the stress distribution shown in Fig. 8, may be represented by the following nondimensional equation:

$$\tilde{P} = \frac{16}{\lambda^3} \tilde{\delta}, \quad (4)$$

where the nondimensional load and the nondimensional mid-span deflection are respectively given by

$$\tilde{P} = \frac{Pl}{\sigma_{c,u} t d^2}, \quad (5a)$$

$$\tilde{\delta} = \frac{\delta l}{\varepsilon_{c,u} d^2}. \quad (5b)$$

The parameter  $l$  is the beam span,  $d$  is the beam effective depth,  $t$  is the beam thickness and  $\lambda$  is the beam slenderness.

Once the ultimate compressive stress,  $\sigma_{c,u}$ , is reached at the extrados, crushing develops in the middle cross-section. Such a nonlinear phenomenon admits the limit configuration shown in Fig. 9. In this situation, two rigid half-beams are connected by a hinge placed at the reinforcement level. The rotational equilibrium is ensured by the applied load, the reaction forces and the linear distribution of the crushing forces. Clearly, this distribution depends on the amount of overlapping: the higher the penetration  $w_c^c$ , the lower the crushing forces until they vanish for  $w_c^c = w_c^c$ .

The rotational equilibrium around point A (see Fig. 9), provides the following nondimensional equation:

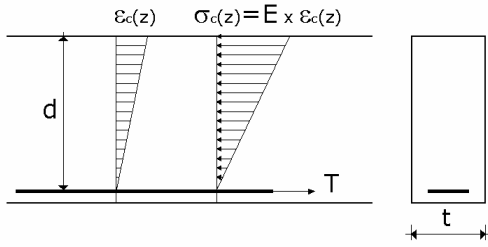


Figure 8. Linear elastic strain and stress distribution.

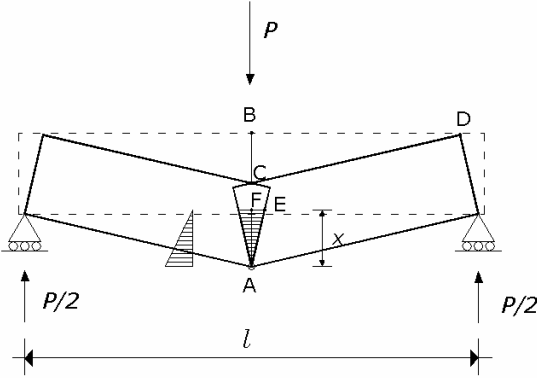


Figure 9. Limit situation of complete overlapping with linear distribution of crushing stresses.

$$\tilde{P} = \frac{1}{6} \left( \frac{s_E^c \lambda^2}{\varepsilon_{c,u} \tilde{\delta}} \right)^2, \quad (6)$$

where

$$s_E^c = \frac{w_c^c}{2d} = \frac{\mathcal{G}_F^c}{\sigma_{c,u} d}. \quad (7)$$

While the linear Eq. (4) describes the mechanical response of the beam in the elastic regime, the hyperbolic Eq. (6) represents the asymptotic behaviour of the beam when it is completely failed in compression.

Figure 10 shows two possible situations. When the domains are separated, the two  $P-\delta$  branches, the linear and the hyperbolic one, may be connected by a regular curve (Fig. 10a). On the other hand, when the two domains are partially overlapped, a snap-back instability may occur (Fig. 10b).

In conclusion, unstable behaviours and catastrophic events are expected when  $\delta_2 \leq \delta_1$ , i.e., for:

$$\frac{s_E^c \lambda^2}{2\varepsilon_{c,u}} \leq \frac{\lambda^3}{12}, \quad (8)$$

which gives the following brittleness condition:

$$\frac{s_E^c}{\varepsilon_{c,u} \lambda} \leq \frac{1}{6}. \quad (9)$$

The mechanical system is expected to be brittle for a low brittleness number,  $s_E^c$ , a high ultimate strain,  $\varepsilon_{c,u}$ , and large slenderness,  $\lambda$ .

It is worth noting that the brittleness condition in Eq. (9), as compared with that obtained for plain

concrete beams, where  $s_E^f/\varepsilon_{t,u}\lambda \leq 1/3$ , (Carpinteri (1989b)) suggests that the crushing phenomenon is more ductile than pure tensile flexural failure.

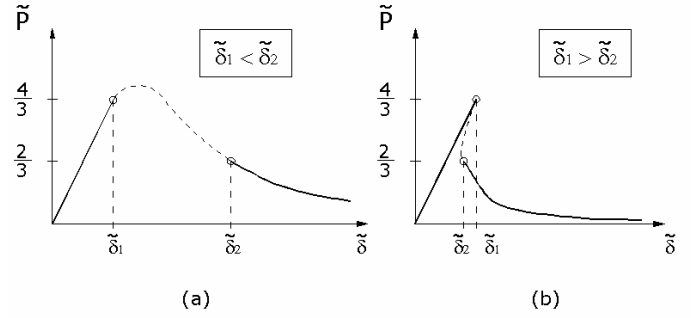


Figure 10. Load - Deflection diagrams: ductile condition (a); brittle condition (b) ( $\delta_1 = \lambda^3/12$ ;  $\delta_2 = s_E^c \lambda^2/2\varepsilon_{c,u}$ ).

## 4 NUMERICAL ALGORITHM

A discrete form of the elastic equations governing the mechanical response of the two half-beams is introduced. To this aim the finite element method is used. At the middle cross-section the nodes of the finite element mesh are distributed along the potential fracture line (nodes from 1 to  $l$ ) and the potential crushing line (nodes from  $l+1$  to  $n$ ) (Fig. 11). The position of the ligament between nodes  $l$  and  $l+1$  is arbitrary; it may depend on the ultimate configuration, i.e. on the material parameters and the reinforcement percentage. In this scheme, cohesive and overlapping stresses are replaced by equivalent nodal forces. They depend on the nodal opening or closing displacements according to the cohesive or overlapping softening laws respectively shown in Fig. 4b and in Fig. 5b.

The horizontal nodal displacements,  $w$ , along the middle cross-section can be computed as follows:

$$\{w\} = [H]\{F\} + \{C\}M \quad (10)$$

where  $\{w\}$  is the vector of nodal displacements,  $[H]$  is the matrix of the coefficients of influence for the nodal forces,  $\{F\}$  is the vector of nodal forces,  $\{C\}$  is the vector of the coefficients of influence for the applied moment and  $M$  is the applied moment.

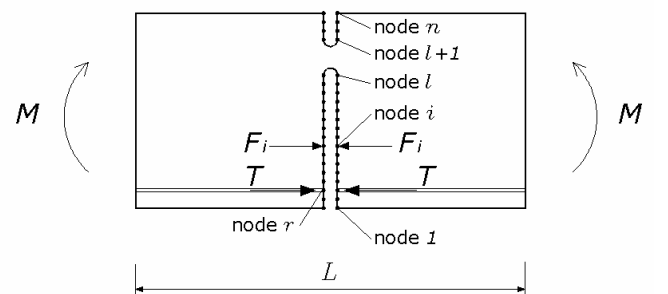


Figure 11. Finite element nodes along potential fracture (1 to  $l$ ) and crushing ( $l+1$  to  $n$ ) lines.

The coefficients of influence representing node opening or overlapping displacements are computed by a finite element analysis in which the fictitious structure shown in Fig. 11 is subjected to  $n + 1$  different loading conditions.

In Eq. (10) the reinforcement contribution is included in the nodal force corresponding to the  $r$ -th node.

In the generic situation shown in Fig. 12a, we can consider the following equations:

$$F_i = 0 \quad \text{for } i = 1, 2, \dots, (j-1); \quad i \neq r \quad (11a)$$

$$F_i = F_{t,u} \left( 1 - \frac{w_i^t}{w_c^t} \right) \quad \text{for } i = j, \dots, (m-1) \quad (11b)$$

$$w_i^t = 0 \quad \text{for } i = m, \dots, n \quad (11c)$$

Equations (10) and (11) constitute a linear algebraic system of  $(2n)$  equations and  $(2n + 1)$  unknowns, i.e., the elements of the vectors  $\{w\}$  and  $\{F\}$  and the applied moment,  $M$ . The additional equation required to solve the problem is obtained by setting the value of the force at the fictitious crack tip,  $m$ , equal to the ultimate tensile force. The driving parameter of the process is the position of the fictitious crack tip, defined by the position of the node  $m$  in Fig. 12a, that is increased by one step at each iteration. The position of the real crack tip,  $j$ , turns out to be a function of the crack opening.

When crushing takes place, (see Fig. 12b), Eqs. 11 are replaced by:

$$F_i = 0 \quad \text{for } i = 1, 2, \dots, (j-1); \quad i \neq r \quad (12a)$$

$$F_i = F_{t,u} \left( 1 - \frac{w_i^t}{w_c^t} \right) \quad \text{for } i = j, \dots, (m-1) \quad (12b)$$

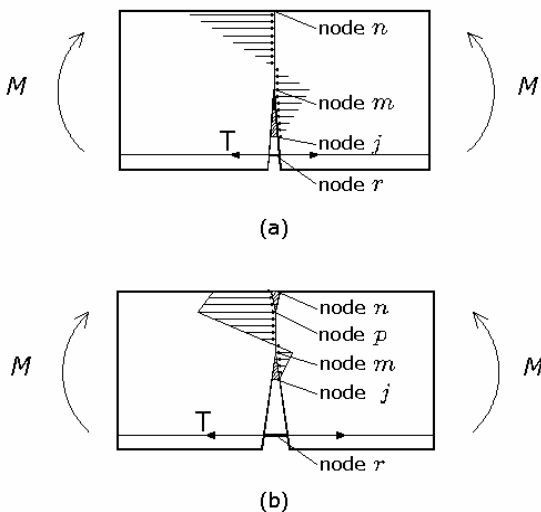


Figure 12. Force distribution with: cohesive crack in tension and linear elastic behaviour in compression (a); cohesive crack in tension and crushing in compression (b).

$$w_i^t = 0 \quad \text{for } i = m, \dots, p \quad (12c)$$

$$F_i = F_{c,u} \left( 1 - \frac{1}{2} \frac{w_i^c}{w_c^c} \right) \quad \text{for } i = (p+1), \dots, n \quad (12d)$$

Again, Equations (10) and (12) constitute a linear algebraic system of  $(2n)$  equations and  $(2n + 1)$  unknowns. In this case, there are two possible additional equations: either the force in the fictitious crack tip,  $m$ , equal to the ultimate tensile force, or the force in the fictitious crushing tip,  $p$ , equal to the ultimate compressive force. In the numerical scheme, we choose the situation which is closer to one of these critical conditions. The driving parameter of the process is the tip that in the considered step has reached the limit resistance. Only this tip is moved passing to the next step.

Finally, at each step of the algorithm it is possible to calculate the beam rotation,  $\vartheta$ , as follows:

$$\vartheta = \{D_F\}^T \{F\} + D_m M \quad (13)$$

where  $\{D_F\}$  is the vector of the coefficients of influence for the nodal forces and  $D_m$  is the coefficient of influence for the applied moment. The physical dimensions of the coefficients  $D_{Fi}$  and  $D_m$  are, respectively,  $[F]^{-1}$  and  $[F]^{-1}[L]^{-1}$ .

## 5 NUMERICAL EXAMPLES

In this section we show the results of numerical simulations carried out to investigate on the influence of two fundamental parameters on the global mechanical behaviour, namely the beam depth and the steel percentage. The midspan cross-section was subdivided into 160 intervals and it was constrained in four nodes. This last region represents the elastic core of the beam at the ultimate condition. In all the following examples the slenderness,  $\lambda$ , and the thickness,  $b$ , are kept constant.

The diagrams depicted in Fig. 13 show the mechanical response in terms of bending moment vs. localised beam rotation, by varying the beam depth for a steel percentage equal to 2%.

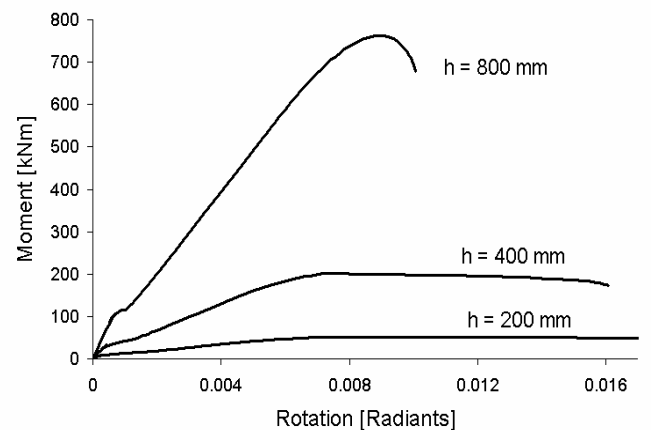


Figure 13. Moment-Rotation diagrams for a constant steel percentage,  $\rho = 2\%$ , and different beam depths,  $h$ .

In the case of  $h = 200$  mm, we have a ductile mechanical response, where the moment-rotation diagram has a first part with positive slope then followed by a plastic flow. Increasing the depth from 200 mm to 400 mm, the plastic range decreases and a softening branch characterized by a low negative slope appears. An analogous behaviour, although more emphasised, is obtained when the depth is equal to 800 mm. Summarizing, we observe that the higher the beam depth, for a given reinforcement ratio, the higher the global stiffness. Obviously, the ultimate resistant moment is an increasing function of the beam depth, whereas the plastic range is progressively diminished with the appearance of steeper and steeper softening branches. The algorithm puts into evidence that the crushing zone increases with the beam depth, while the crack opening at the intrados decreases.

Another set of simulations was carried out by considering a constant beam depth equal to 400 mm and by varying the reinforcement ratio from 0.12% to 3%. The resulting moment-rotation diagrams are shown in Fig. 14. According to the numerical and experimental results concerning the minimum reinforcement in RC beams (see Bosco et al. (1990), Bosco and Carpinteri (1992)), the global behaviour with a very low steel percentage (e.g. 0.12%) is brittle. By increasing the steel ratio, two transitions may be highlighted. From  $\rho = 0.12\%$  to  $\rho = 1\%$  we have a transition from brittle to ductile and then, from  $\rho = 1\%$  to  $\rho = 3\%$ , the mechanical behaviour becomes brittle again. For the highest reinforcement ratio, a softening branch occurs due to concrete crushing. In Figs. 15 and 16 we see that for a very low steel percentage ( $\rho = 0.12\%$ ) the ultimate resistant moment is provided by a tensile plastic flow in the reinforcement and a compressive zone concentrated in the extrados. In this case the ductile behaviour is due to the reinforcement yielding. With  $\rho = 1\%$ , the reinforcement is yielded at the ultimate condition, but a lower value of crack opening is observed. On the other hand, the crushing contribution becomes more relevant.

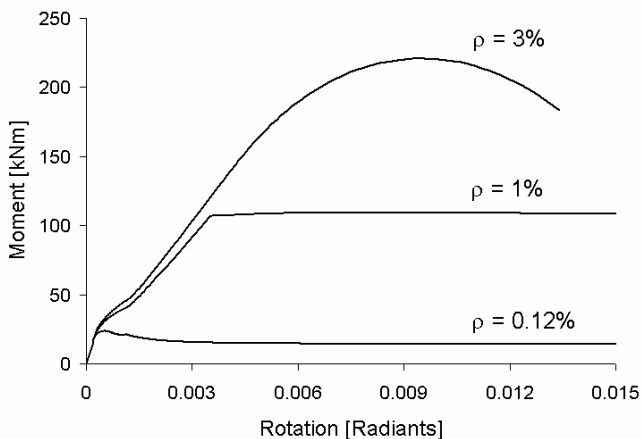


Figure 14. Moment-Rotation diagrams for a constant beam depth,  $h = 400$  mm, and different steel percentages,  $\rho$ .

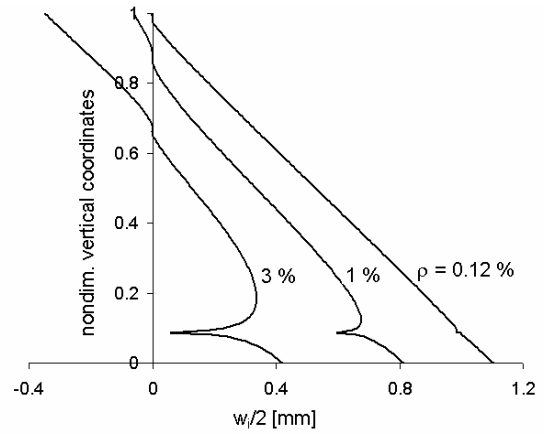


Figure 15. Horizontal nodal displacements for a constant beam depth,  $h = 400$  mm, and different steel percentages,  $\rho$ , at the ultimate condition.

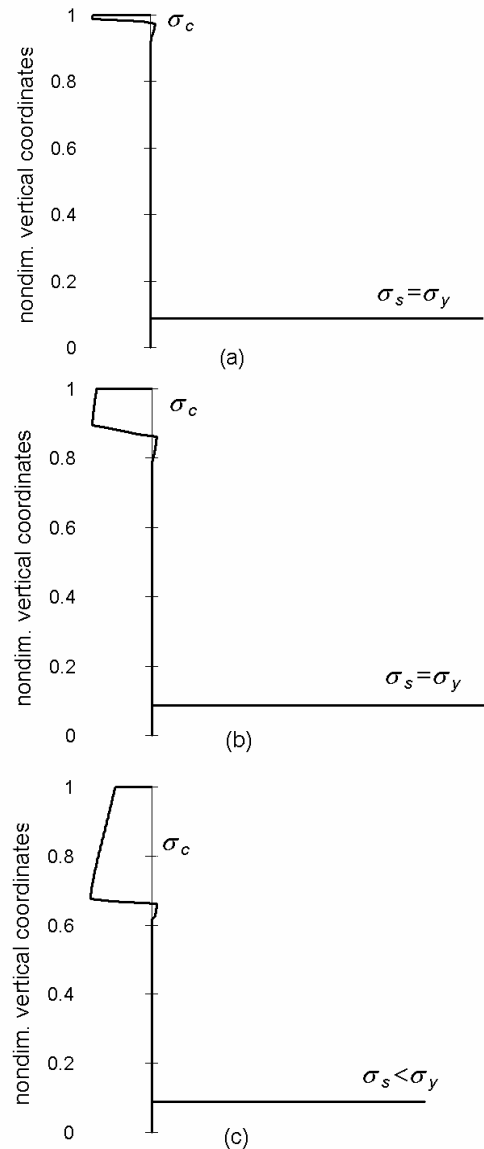


Figure 16. Stress distribution at the ultimate condition referred to:  $\rho = 0.12\%$  (a),  $\rho = 1\%$  (b),  $\rho = 3\%$  (c) ( $h = 400$  mm).

For a very high steel percentage ( $\rho = 3\%$ ) the reinforcement is not yielded and so the only contribution to the ductility results from crushing. In this situation the ultimate resistant moment is not proportional to the reinforcement ratio, because it is limited by the maximum compressive force.

Finally, it is worth noting that, in the case of low steel percentages, crushing does not take place and a single nondimensional parameter,  $N_p$  (Carpinteri (1981) and (1984)) can be used to describe the transition from ductile to brittle behaviours:

$$N_p = \frac{\rho \sigma_y h^{0.5}}{\sqrt{\mathcal{E}_F E_c}} \quad (14)$$

A brittle to ductile transition clearly emerges in the diagrams of Fig. 17, when the brittleness number increases. The diagrams reveal an unstable response, represented by a strain-softening relationship, for the lower brittleness number, and a stable response, represented by a strain-hardening relationship, for the higher brittleness number.

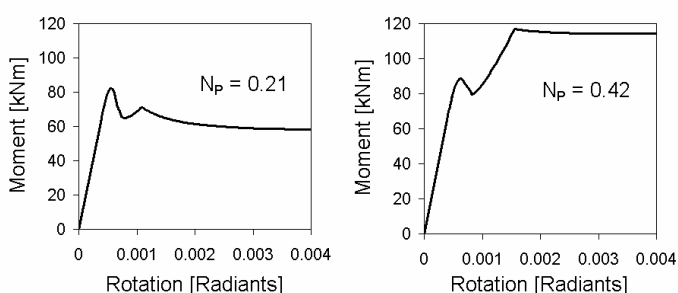


Figure 17. Moment-Rotation diagrams for a low reinforcement ratio,  $\rho = 0.25\%$ , and two different brittleness numbers,  $N_p$ .

## 6 CONCLUSIONS

In this paper we have proposed a new mathematical and numerical approach to the problem of crushing in RC beams, which is treated in analogy with the cohesive formulation. The effect of the reinforcement contribution, which is not usually included in the cohesive models, has been taken into account as a local modification of the tensile cohesive law.

This very general approach has permitted to investigate on the competition between compressive crushing and tensile cracking in RC beams, with special focus on size-scale effects. Future developments are expected as far as the analysis of the size effects on the rotational capacity is concerned. In this framework, a comparison with the experimental results in Bosco, Carpinteri and Debernardi (1992) will be proposed.

## ACKNOWLEDGEMENTS

The financial support provided by the Ministry of University and Research (MIUR) is gratefully acknowledged.

## REFERENCES

- Bosco, C., & Carpinteri, A. 1992. Softening and snap-through behavior of reinforced elements. *Journal of Engineering Mechanics (ASCE)*, Vol. 118, 1564-1577.
- Bosco, C., Carpinteri, A. & Debernardi, P.G. 1990. Minimum reinforcement in high strength concrete. *Journal of Structural Engineering (ASCE)*, Vol. 116, 427-437.
- Bosco, C., Carpinteri, A. & Debernardi, P.G. 1992. Scale effect on plastic rotational capacity of R.C. beams. In *Fracture Mechanics of Concrete Structures* (Proceedings of the 1st FraMCoS Conference, Breckenridge, USA, 1992), Ed. Z.P. Bazant, Elsevier Applied Science, London, 735-740.
- Carpinteri, A. 1981. A fracture mechanics model for reinforced concrete collapse. In *Advanced Mechanics of Reinforced Concrete* (Proceedings of a IABSE Colloquium, Delft, the Netherlands, 1981), Delft University Press, Delft, 17-30.
- Carpinteri, A. 1984. Stability of fracturing process in R.C. beam. *Journal of Structural Engineering (ASCE)*, Vol. 110, 544-558.
- Carpinteri, A. 1986. Limit analysis for elastic-softening structures: scale and slenderness influence on the global brittleness. In *Structure and Crack Propagation in Brittle Matrix Composite Materials* (Proceedings of the Euromech Colloquium 204, Warsaw, Poland, 1985), Eds. A. M. Brandt, I. H. Marshall, Elsevier Applied Science, London, 497-508.
- Carpinteri, A. 1989a. Cusp catastrophe interpretation of fracture instability. *Journal of the Mechanics and Physics of Solids*, Vol. 37, 567-582.
- Carpinteri, A. 1989b. Size effects on strength, toughness, and ductility. *Journal of Engineering Mechanics (ASCE)*, Vol. 115, No. 7, July, 1375-1392.
- Carpinteri, A., Di Tommaso, A. & Fanelli, M. 1985. Influence of material parameters and geometry on cohesive crack propagation. In *Fracture Toughness and Fracture Energy of Concrete*, (Proceedings of an International Conference on Fracture Mechanics of Concrete, Lausanne, Switzerland, 1985), Ed. F.H. Wittmann, Elsevier, Amsterdam, The Netherlands, 117-135.
- Carpinteri, A. (ed.) 1999. *Minimum Reinforcement in Concrete Members*, Elsevier Science Ltd, VIII + 203, Oxford, UK.
- Carpinteri, A., Ferro, G. & Ventura, G. 2005. Scale-independent constitutive law for concrete in compression. *Proceeding of the 11<sup>th</sup> International Conference on Fracture (ICF)*, Torino, Italy, 2005, CD-ROM, Paper N. 5556.
- Comité Euro-International du Béton. 1993. CEB-FIP Model Code 1990.
- Hillerborg, A. 1990. Fracture mechanics concepts applied to moment capacity and rotational capacity of reinforced concrete beams. *Engineering Fracture Mechanics*, Vol. 35, 233-240.
- Hillerborg, A., Modeer, M. & Petersson, P. E. 1976. Analysis of crack formation and crack growth in concrete by means of fracture mechanics and finite elements. *Cement and Concrete Research*, Vol. 6, 773-782.
- Jenq, Y. S. & Shah, S. P. 1989. Shear resistance of reinforced concrete beams – a fracture mechanics approach. In *Fracture Mechanics: Application to Concrete* (Special Report ACI SP-118), eds. Li, V. C. and Bazant, Z. P., American Concrete Institute, Detroit, 327-358.
- Suzuki, M., Akiyama, M., Matsuzaki, H. & Dang, T.H. 2006. Concentric loading test of RC columns with normal- and high-strength materials and averaged stress-strain model for confined concrete considering compressive fracture energy. In *FIB, Proceedings of the 2<sup>nd</sup> International Conference*, June 5-8, 2006 – Naples, Italy.
- Van Vliet, M. & Van Mier, J. 1996. Experimental investigation of concrete fracture under uniaxial compression. *Mechanics of Cohesive-Frictional Materials*, Vol. 1, 112-127.